Available online at www.sciencedirect.com
ScienceDirect
Trans. Nonferrous Met. Soc. China 20(2010) 34−42
Transactions of Nonferrous Metals Society of China
www.tnmsc.cn

Friction stir processing of thixoformed AZ91D magnesium alloy and fabrication of Al-rich surface

CHEN Ti-jun(陈体军), ZHU Zhan-ming(朱战民), LI Yuan-dong(李元东), MA Ying(马 颖), HAO Yuan(郝 远)

State Key Laboratory of Gansu Advanced Nonferrous Materials,
Lanzhou University of Technology, Lanzhou 730050, China

Received 14 November 2008; accepted 10 March 2009

Abstract: The microstructural evolution characteristics of thermo-mechanically affected zone were investigated during friction stir processing (FSP) of the thixoformed AZ91D alloy. Simultaneously, an Al-rich surface layer was prepared by combination of Al powder using FSP method. The results indicate that the dynamic recrystallization and mechanical separation (including splitting and fracture of the primary grains) are the main mechanisms of grain refinement. For the thixoformed alloy, the operation efficiency of these mechanisms is less than that of the permanent mould casting AZ91D alloy, thus its microstructural evolution is relatively slow and the resulting grain size is relatively large. These are attributed to the differences in their original microstructures. The Al-rich surface layer can obviously improve the corrosion resistance in NaCl aqueous solution. A proper solution heat treatment (at 415 ℃ for 1 h) can further increase the corrosion resistance. In order to improve corrosion resistance, increasing the amount and improving the distribution uniformity of the Al-rich phase are more effective than increasing the Al solubility in the matrix.
Key words: AZ91D alloy; Al-rich surface layer; friction stir processing; thixoforming; corrosion resistance

1 Introduction

Magnesium alloys present a great potential as structural materials in the aerospace and automobile industries because of several advantages, such as low density, high specific strength and good machinability[1]. However, AZ91D alloy, one of the most common commercial magnesium alloys, suffers from the challenge in meeting the requirements of strength, ductility and creep resistance[2]. In order to improve these properties, thixoforming has been adapted to produce components with a unique microstructure with small spherical primary particles uniformly distributed in the matrix, which is essentially different from those produced by using conventional casting techniques[2−3]. Unfortunately, compared with some commonly-used metal materials, such as Al, Cu and Fe alloys, magnesium alloys prepared by either traditional casting or thixoforming always have poor specific elongation due to the hexagonal close-packed structure and low corrosion resistance due to the high chemical activities[4−7]. The former shortcoming can be overcome by grain refinement while the latter one can be improved by increasing Al concentration in the α phase or amount of the uniformly distributed β phase ($Mg_{17}Al_{12}$)[8−10].

Friction stir processing (FSP) is a relatively new technique for microstructural modification of metal materials invented by CHARIT and MISHRA[11] based on the principles of friction stir welding. In FSP, a rotating tool is inserted into a material and produces a high plastic deformation. An ultrafine grain structure can be obtained by dynamic recrystallization of the deformed zone. So, FSP has been used to prepare Al and Mg alloys with ultrafine grains. The results indicated that for the FSPed magnesium alloys, the grain size could be decreased to a few micrometers and the mechanical properties were significantly improved[12−16]. Furthermore, FSP has also been used to fabricate surface composites reinforced by intermetallic particles, SiC particles, SiO_2 particles, C_{60} molecules or fullerene on

Foundation item: Project(2007CB613706) supported by the National Basic Research Program of China; Project(3ZS042-B25-003) supported by the Natural Science Foundation of Gansu Province, China; Project(SKL03004) supported by the Development Program for Outstanding Young Teachers in Lanzhou University of Technology, China
Corresponding author: CHEN Ti-jun; Tel: +86-931-2976573; E-mail: chentj1971@126.com; chentj@lut.cn
DOI: 10.1016/S1003-6326(09)60093-5

traditional cast Al or Mg alloy substrates[17−27].

From the above description, it can be found that the grain refinement by FSP has focused on some traditional casting Mg or Al alloys and less investigation has involved the thixoformed alloys. However, the microstructures of the alloys prepared by these two techniques are significantly different and thus the microstructural evolutions have their respective characteristics. In addition, enlightened from the fabricating surface composites by FSP, it can be expected that an Al-rich surface on Mg alloys can be prepared by using FSP so that their corrosion resistance will be improved. Therefore, in this work, the microstructural evolution characteristics of the thermo-mechanically affected zone were discussed during FSP of thixoformed AZ91D Mg alloy and an Al-rich surface was prepared by FSP. Correspondingly, the corrosion resistance in NaCl aqueous solution was also examined.

As discussed above, the corrosion resistance of Mg alloys can be improved by increasing Al solubility in α-Mg phase[8−10]. But in the present alloy, part of Al element might be in the form of pure Al particles because the Al element was incorporated with the AZ91D alloy by mechanical stirring in terms of Al powder. To make the Al element uniformly distribute and to increase the Al solubility in the α-Mg matrix, a solution heat treatment can be used. So, in this work, the effects of solution treat treatment on the microstructure and corrosion resistance of the Al-rich surface AZ91D alloy were also discussed.

2 Experimental

The alloy used in this work was commercial AZ91D alloy ingots. A quantity of the AZ91D alloy was remelted at 720 ℃ and poured into a steel mould to form some rods with 45 mm in diameter. These rods were cut into short rods with 85 mm in length as the starting ingots for thixoforming. Each short rod was heated for 90 min at a semisolid temperature of 585 ℃ in a muffle furnace and then handled in a die and pressed under a 200 MPa pressure. Consequently, a thixoformed AZ91D plate with dimensions of 100 mm×40 mm×15 mm was obtained. Repeating this process, some thixoformed (TF) plates were formed. For comparison, several traditional permanent mould casting (PMC) plates with dimensions of 200 mm×200 mm×15 mm were also prepared (AZ91D melt at 720 ℃ was poured into a steel mould with ambient temperature).

FSP was carried out on the surfaces of the above plates by using FSW−3LM−015 friction stir welder. A tool pin with height of 5 mm and diameter of 7 mm was used. The shoulder diameter was 20 mm, and a 3°-tilt angle for the fixed pin tool was applied. A constant tool rotating rate of 450 r/min was adopted, and the rotating tool was traversed at a speed of 60 mm/min along the long axis of the plates. To verify the effect of FSP pass on the microstructures and deduce the microstructural evolution, multiple FSP passes were applied along the same line. The FSPed plates were cross-sectioned perpendicular to the welding direction, polished and then etched with 4% HNO_3 aqueous solution. Microstructural features were characterized by optical microscope (OM). The average grain size was measured by a quantitative microstructural analysis system equipped with the OM.

For preparing an Al-rich surface layer, commercially available Al powder (mean diameter of 10 μm) was used. Three grooves with 4.2 mm in depth and 1.25 mm in width were machined on a plate along the long axis. The distance between the grooves was 6 mm. The Al powder was filled into the grooves. The tool used in this section has a shoulder with diameter of 18 mm and a pin with diameter of 6 mm and length of 4 mm. The pin was inserted into the groove filled with the Al powder. A constant tool rotating rate of 350 r/min was adopted, and the rotating tool was traversed at a speed of 45 mm/min along the groove. The tool tilt angle of 3° was used. After the three grooves were FSPed, the microstructure was characterized by scanning electron microscope (SEM) and electron probe micro-analyzer (EPMA) on the cross-section of the FSP sample. In order to verify the effect of combination of Al powder on corrosion resistance, the stirred zone (about 3.5 mm in thickness) was cut parallel to the stirred surface and divided into some small specimens (12 mm×12 mm×3.5 mm). One specimen was finished and polished, and then immersed into 10% NaCl aqueous solution for 6 h (because the Al-based materials have relatively high corrosion resistance, the concentration of NaCl in the solution was increased from 3.5% to 10% in order to accelerate the corrosion rate and decrease the testing time). The average mass-loss ($mg\cdot cm^{-2}\cdot h^{-1}$)) was taken as the corrosion rate. The other specimens were solution heat treated for different durations, ranging from 1 h to 4 h at 415 ℃, and then their microstructures and corrosion resistance were examined. The as-received and heat treated Al-rich surface layers were analyzed by X-ray diffractometer (XRD) and energy-dispersive spectrometer(EDS) in order to verify the status of the combined Al powder and the effect of the solution heat treatment.

3 Results and discussion

3.1 Microstructural evolution characteristics during FSP

3.1.1 Microstructure characteristics of as-received alloys

In order to verify the microstructural evolution

characteristics during FSP, the original microstructures of the as-thixoformed (TF) and permanent mould cast (PMC) alloys should be firstly observed. Fig.1 shows the microstructures of both the TF and PMC alloys. It can be found that the microstructures of these two alloys are completely different. The microstructure of the TF alloy consists of spherical primary α phase particles and intergranular secondarily solidified structure (solidified from the liquid phase in semisolid ingot prior to thixoforming) (Fig.1(a)). The primary particle size is relatively large with an average size of about 120 μm while the secondarily solidified structure is very fine due to rapid solidification during thixoforming. Some black particles can be found in the primary particles and they solidify from the liquid pools entrapped within the primary particles at semisolid state, i.e. they also belong to the secondarily solidified structure[28]. However, the microstructure of the PMC alloy is composed of primary equiaxed α phase dendrites and eutectic structure that distributes in the inter-dendrites in a continuous network form (Fig.1(b)). The average size of the dendrites is about 100 μm. It can be seen that the size of the primary grains (particles) of the TF alloy is larger than that of the PMC alloy. Generally, the structure of TF alloys should be smaller than that of the traditional PMC alloys[29]. The reverse result of this work results from the fact that the thickness of the PMC plates is relatively small (15 mm) and a fine equiaxed dendritic structure can easily form during solidification due to strong chilling of the steel mould used[30].

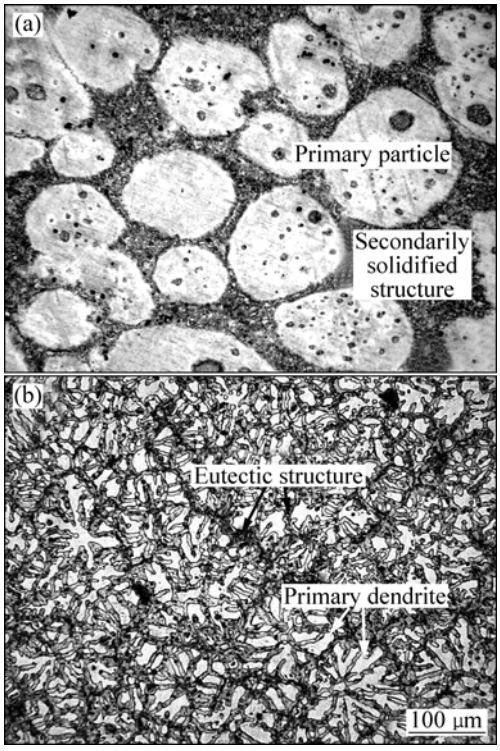

Fig.1 OM micrographs of TF (a) and PMC (b) AZ91D alloys

For the TF alloy, the secondarily solidified structure includes secondarily primary phase (to differentiate from the primary particles, the primary phase solidified from the liquid phase in the semisolid state is named secondarily primary phase) and eutectic structure (Fig.2(a)). The eutectic structure is very fine. But for the PMC alloy, the eutectic structure is relatively coarse, and only the large eutectic β phase that macroscopically uniformly distributes in inter-dendrites or inter-dendritic arms can be distinguished while the eutectic α phase fuses with the primary dendrites (Fig.2(b)). This implies that this eutectic structure is divorced eutectic.

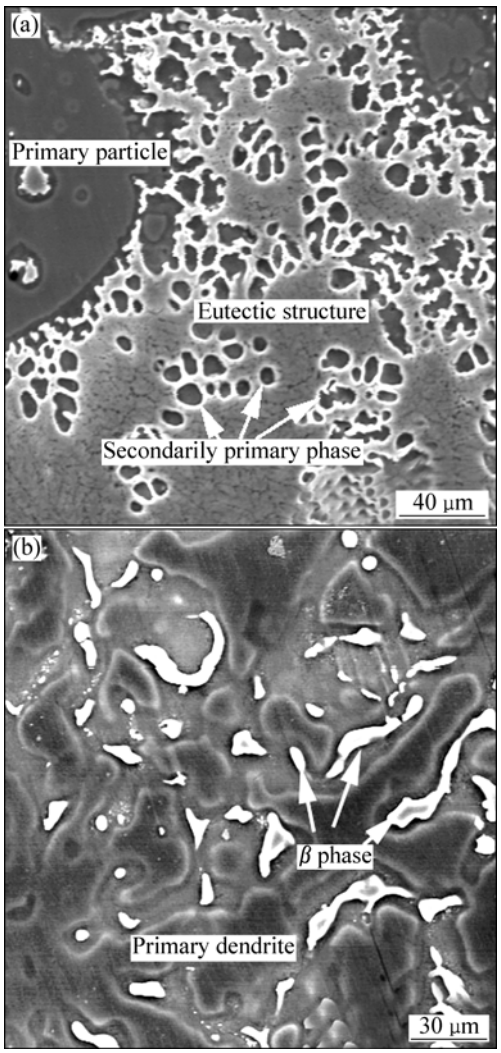

Fig.2 SEM micrographs of TF (a) and PMC (b) AZ91D alloys

3.1.2 Microstructural evolution characteristics of thermo-mechanically affected zone during FSP

The mechanism of grain refinement of FSP belongs to sever plastic deformation induced grain refinement [11−15]. In order to verify the details of this kind of grain refining mechanism, a method that has been frequently accepted is to study the microstructural evolution with the increase of strain during processing.

For the FSPed alloy, as shown in Fig.3, four distinct zones, stirred zone (SZ), thermo-mechanically affected zone (TMAZ), heat-affected zone (HAZ) and parent material (PM) can be found. Although the strain in the SZ increases with the increase of stir pass, the strain generated in one pass is so large that the deformation process is difficult to be obviously observed. However, for the TMAZ, it is not only affected by heat, but also affected by strain, relatively similar to the status of the SZ although the detailed conditions between these two zones are significantly different[31]. So, the study on the TMAZ can provide important information for verifying the microstructural evolution of the SZ during FSP. In the TMAZ, both the strain and heat continuously increase as the stir pass increases, and thus the microstructural evolution of the material in the TMAZ with stir pass can be relatively easily verified.

Fig.4 shows the micrographs of the TMAZs of the TF alloys FSPed for different stir passes. By comparing Fig.4(a) with Fig.1(a), it can be seen that the primary particles are elongated after being processed for 2 passes. As the processing pass increases, the primary particles become longer and longer and gradually evolve into thin strips (Fig.4(b)). Simultaneously, it can be found that the number of the strips significantly increases compared with that of the primary particles in a given visual field (by comparing Fig.1(a) or 4(a) with 4(b)). One reason is that the primary particles in the other field are elongated and extended to this field. The other is that there is multiplication phenomenon for the particles during being elongated. As shown by arrows A in Fig.4(a), the elongated primary particles are branched and it can be expected that the secondarily solidified structure existing between the branches would split them into two parts during the subsequent elongation. Similarly, as shown by arrow B, the spherical black particles within the primary particles could also play a role of splitting. In addition, it is also found that the strips are not continuous and integrated, but are composed of lots of small-size columns (Fig.4(d)). This implies that the long primary strips dynamically recrystallize during processing, and of course, it is possible that they are mechanically separated into short columns when the strain exceeds their fracture utmost. When the pass is further increased, due to the mechanical fragmentation (including splitting and fracture) and dynamic recrystallization, the small-size columns gradually evolve into very fine particles (Fig.4(c)), a microstructure similar to that of the

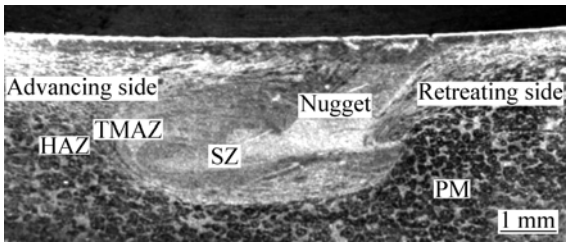

Fig.3 Cross-sectional OM macrograph of TF AZ91D alloy FSPed for four passes

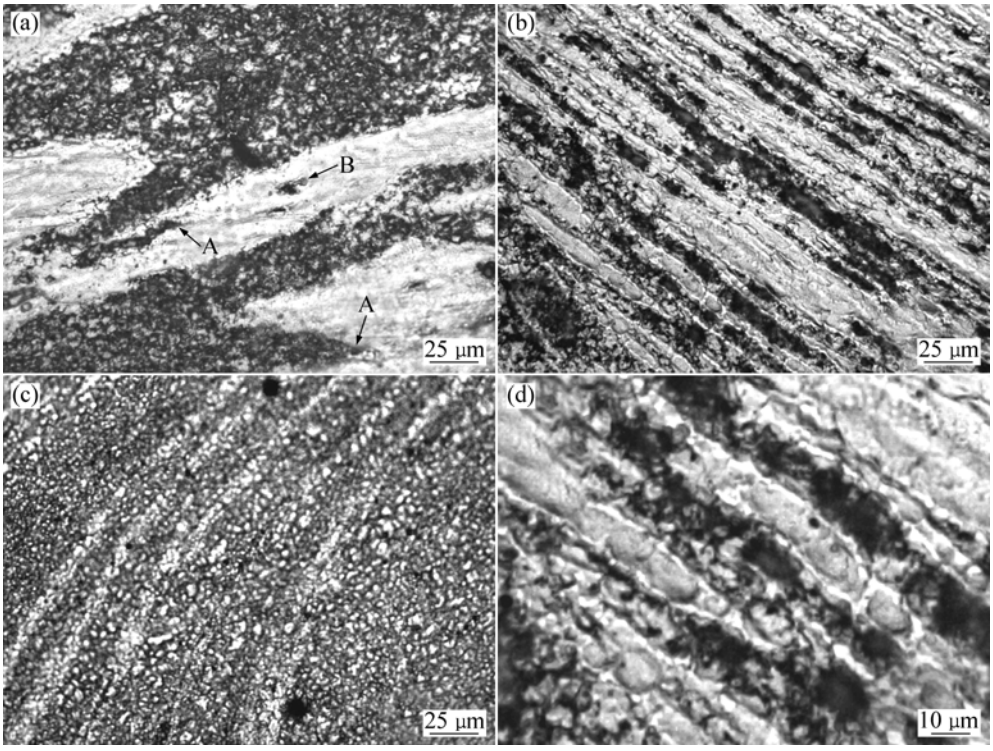

Fig.4 OM micrographs of TMAZs of TF AZ91D alloys FSPed for different passes: (a) 2; (b) 4; (c) 6; (d) Large magnification micrograph of (b)

SZ (Fig.5(a)).

Fig.5 shows the microstructures of the SZs of the TF and PMC AZ91D alloys FSPed for 6 passes. It is indicated that a fine-grained microstructure can be obtained for both the TF and PMC alloys after being FSPed. Their grain sizes are also very similar (by comparing Fig.5(a) with 5(b)). However, there are differences in the microstructure characteristics of TMAZs at a given stir pass and in the grain size of SZs when being FSPed for less passes.

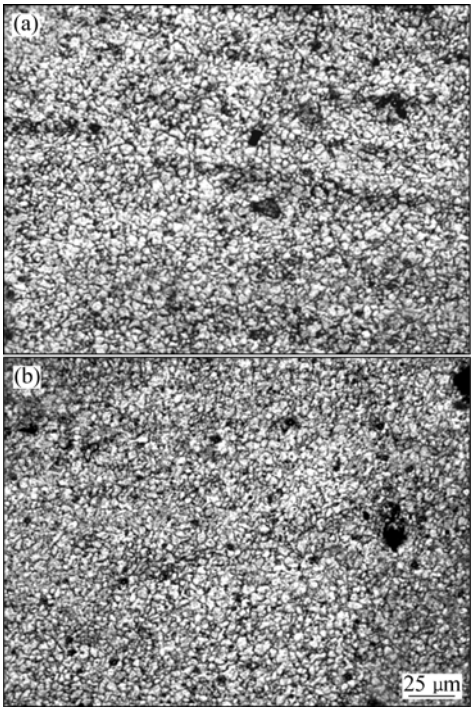

Fig.5 OM micrographs of nuggets of TF (a) and PMC (b) AZ91D alloys FSPed for 6 passes

Fig.6 presents the micrographs of the TMAZs of the PMC alloys FSPed for different passes. Compared with the corresponding micrographs of TF alloy shown in Fig.4, it can be found that the dendrites, similar to the primary particles of TF alloy, are also plastically deformed along the stir direction and become into a directional grain structure after being processed for 2 passes (Fig.6(a)). When the stir pass is increased to 4, the elongated dendrites or dendritic arms evolve into fine equiaxed particles (Fig.6(b)). The grain size is slightly smaller than that of the corresponding TF alloy and the material flow line is also more blurry (by comparing Figs.6(b) with 4(b)). As the pass increases to 6, the grain size further decreases and the flow lines almost disappear, very similar to the structure of the SZ (by comparing Figs.6(c) with 5(b)). By comparing the microstructural characteristics of these two alloys, it can be found that the microstructural evolution of the PMC alloy with the stir pass is quicker than that of the TF alloy and the grain refinement of the FSP is more effective for the dendritic PMC alloy. However, it should be noted that

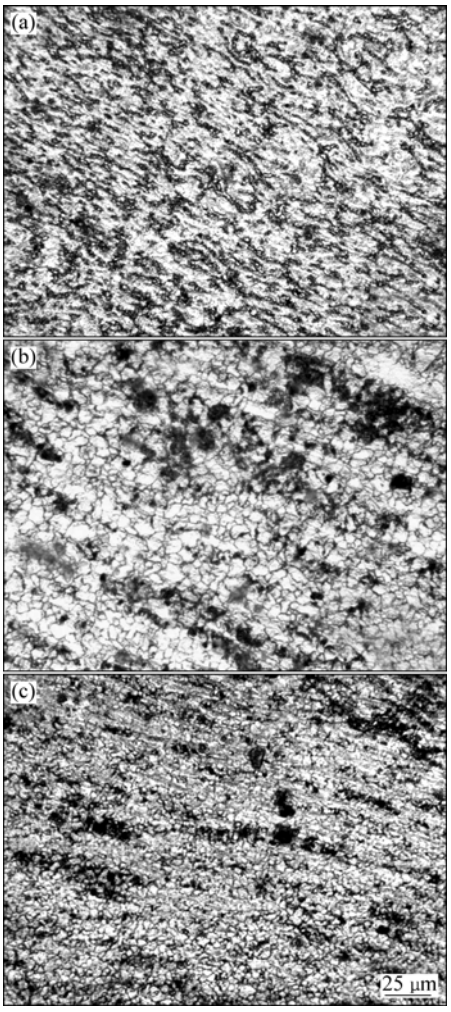

Fig.6 OM micrographs of TMAZs of PMC AZ91D alloys FSPed for 2 (a), 4 (b) and 6 (c) passes

the microstructural evolution process can be more obviously observed for the IF alloy because of its large spherical grains. That is to say, the unique microstructure of the TF alloy is beneficial for verifying the microstructural evolution during FSP.

As discussed above, the mechanical separation and dynamic recrystallization are the main reasons for grain refinement. Based on their individual mechanisms, it can be proposed that the mechanical separation related to the splitting of primary grains is mainly determined by the distribution of eutectic structure, i.e., it is essentially related to the morphology of primary phase. The mechanical separation related to the fracture of the elongated primary grains is mainly dependent on the strain while the dynamic recrystallization is affected by both the strain and heat. For the TF alloy, most of the eutectics agglomerate in the relatively large zones among the spherical primary particles (Fig.2(a)). But for the PMC alloy, the devoiced eutectic β phase uniformly distributes in the inter-dendrites or inter-dendritic arms (Fig.2(b)). The eutectic or β phase is relatively hard and difficult to deform while the primary phase (including

primary particles and dendrites) is soft and easy to deform[28, 32]. When the primary phase is plastically deformed along a direction during FSP, the hard eutectic or β phase can prevent the primary phase from deformation and makes them generate some breaches (also branches in Fig.4(a)), and finally splits them into several parts with the increase in stir pass. It can be expected that the more uniform the distribution of eutectic or β phase, the more the number of the resulting primary phase strips. In addition, the strain generated in the primary phase is larger for the alloy with more uniform distribution of the eutectics or β phases at a given stir pass (i.e. a given general strain) because the volume of the primary phase between the eutectic and β phase is small. Furthermore, the heat generated from friction is also large for this alloy. Thus, both the dynamic recrystallization and mechanical separation are easier to operate. Based on these standpoints, it can be concluded that the mechanical separation and dynamic recrystallization are all easier to operate for the PMC alloy than the TF alloy. So, the microstructural evolution of the PMC alloy with the stir pass is quicker than that of the TF alloy and the resulting grain size is also finer (Fig.5). Of course, it is not neglected that the original primary grain size of the as-cast PMC alloy is smaller than that of the as-thixoformed TF alloy.

Fig.7 quantitatively presents the grain sizes in the SZs of the PMC and TF alloys FSPed for different passes. It is shown that the grain size of the TF alloy is larger than that of the PMC alloy when the stir pass is relatively few. The difference between them decreases as the stir pass increases and they become equivalent after being stirred for 6 passes. From the grain refinement mechanisms discussed above, it can be found that the microstructure differences in the TMAZs of these two alloys decrease as the stir pass increases due to severe plastic deformation (by comparing the corresponding micrographs shown in Figs.4 and 6). That is to say, the effect resulted from the differences in the original as-cast or thixoformed microstructures decreases as the stir pass increases.

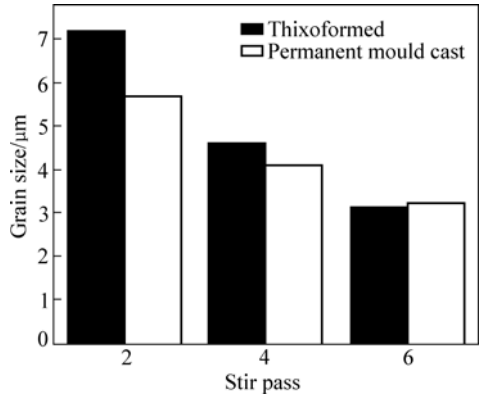

Fig.7 Variations of grain sizes of TF and PMC AZ91D alloys with stir pass

3.2 Al-rich surface layer and corrosion resistance

3.2.1 As-received microstructures and corrosion resistance

The general microstructure characteristics and corrosion resistance of the Al-rich surface layers of both the TF and PMC alloys are very similar although there are some differences in the microstructures of the TMAZs and SZs of these alloys especially being FSPed for few passes. Therefore, only the results about the TF alloy are presented. Fig.8 shows the microstructure of the Al-rich surface. This indicates that a large number of white particles distribute along the material flow lines. The results from EPMA show that these white particles are Al-rich phase (Fig.9). The XRD results indicate that

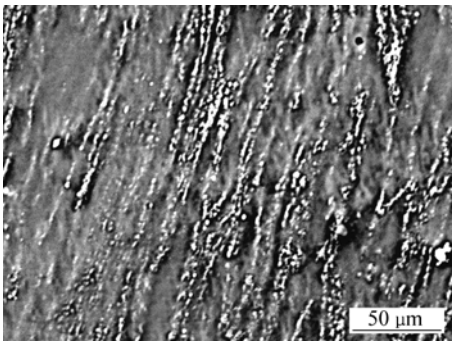

Fig.8 SEM micrograph of Al-rich surface layer of TF alloy

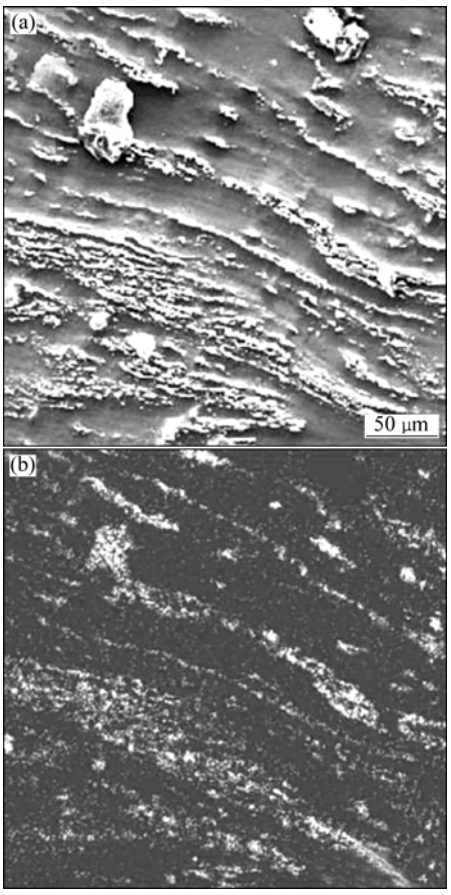

Fig.9 SEM micrograph (a) and distribution of Al (b) of Al-rich surface layer resulted from EPMA

there is pure Al phase besides the α-Mg and β phases (by comparing the XRD spectrum of the thixoformed alloy with that of the FSPed with Al shown in Fig. 10). But the further examination by EPMA indicates that the pure Al phase is completely mixed with the β phase and it is difficult to distinguish them. This implies that a part of the Al powder transforms into β phase driven by the friction heat. Therefore, it can be concluded that the distribution of the combined Al element is macroscopically uniform in the surface layer, but is not uniform in micro-scale, and a part of the Al powder transfers into β phase during FSP.

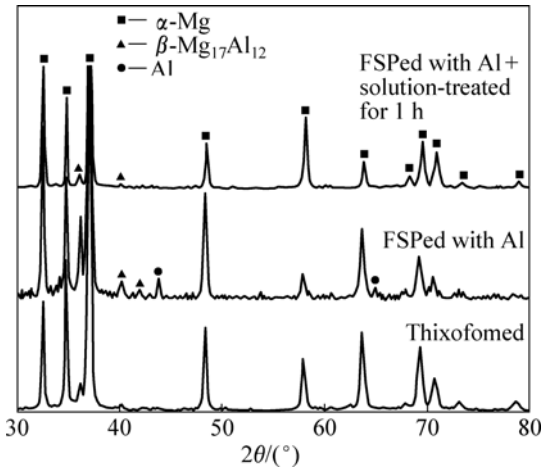

Fig.10 XRD patterns of TF alloys

The average Al content in the surface layer increases although the distribution of Al element is not uniform. The present results show that the average corrosion rate of the alloy with such Al-rich surface in 10% NaCl solution is about 0.429 mg/(cm^2·h) while that of the thixoformed alloy is about 0.549 mg/(cm^2·h), i.e., the corrosion resistance of the Al-rich surface is increased by about 22% compared with that of the thixoformed alloy. This increase in corrosion resistance should be attributed to two factors. One is the increase of Al solubility in the α-Mg matrix. A previous investigation showed that the Al solubility in the primary α particles was about 3.5% (mass fraction) for the thixoformed AZ91D alloy[7], but the present EDS result shows that the solubility in the α matrix is 8.32% (mass fraction) for the Al-rich surface layer produced by FSP. The increase of the Al solubility results from the dissolution of either the β phase or the pure Al due to the rise of temperature during FSP, which can improve the corrosion resistance[9]. The other is the increased barrier role from the β phase and pure Al phase. SONG et al[10] proposed that increasing the amount of β phase and improving its distribution uniformity could obviously increase the corrosion resistance of AZ91D alloy. But for the pure Al, it is well known that it has better corrosion resistance than Mg, so, similar to the β phase, it can also play a barrier role. After being FSPed with Al powder, the total amount of the β phase and pure Al phase increases, thus the corrosion resistance increases. It must be noted that the combination of Al powder would increase the number of galvanic cell, thus decrease the corrosion resistance. But the present results indicate that the benefit of the combination of Al powder to the corrosion resistance is larger than the harm.

3.2.2 Effects of heat treatment on microstructure and corrosion resistance

From the above discussion, it can be found that the distribution of the combined Al element in the surface layer is quite non-uniform and is mainly concentrated along the material flow lines. In order to improve the distribution uniformity and further enhance the corrosion resistance, solution heat treatment was carried out. Fig.11 gives the microstructures of the surface layers heat treated at 415 ℃ for different durations. It can be

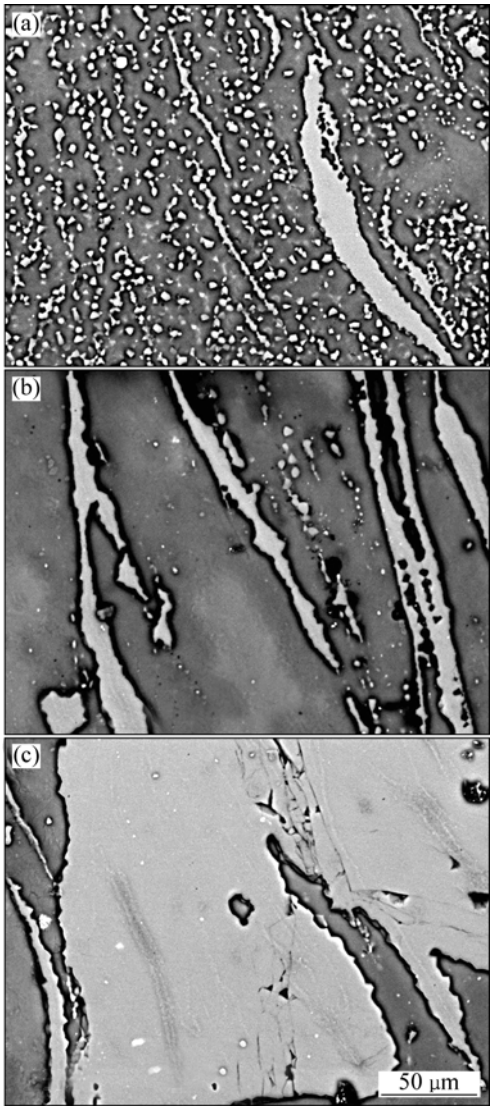

Fig.11 SEM micrographs of Al-rich surface layers solution-treated at 415 ℃ for 1 h (a), 2 h (b) and 4 h (c)

seen that the Al-rich phases (including β phase and pure Al phase) tend to spheroidize and they change from the original continuous line distribution along the material flow lines (Fig.8) into the individual small particles with quite uniform distribution after being treated for 1 h (Fig.11(a)). However, the original cluster-distributed Al-rich phases present in the long and large strip structure. As the heat time is prolonged, all of the Al-rich phases further agglomerate and turn into long strips (Fig.11(b)), and finally become into large slice structure when the treating time is up to 4 h (Fig.11(c)). The microstructure has no obvious change when the heating time exceeds 4 h. The observation results also show that the large slices are always in the center of the SZs and can be seen by naked eye. Besides the large slices, there is almost no Al-rich phase in most of the areas.

The XRD patterns indicate that all of the residual pure Al phases transform into β phase when being solution-treated for 1 h (Fig.10) and no transformation occurs after then. So, it can be concluded that all of the Al-rich phases shown in Fig.11 are β phase. It is also found that the Al solubility (examined by EDS) in the matrix continuously increases due to the dissolution of the Al-rich phase (referring to the β phase after being heated for 1 h) with the increase of heating duration (Fig.12). It is obvious that a large amount of the combined Al powder still presents in agglomerated state, i.e. β phase, although considerable powder dissolves into the α matrix after heat treatment.

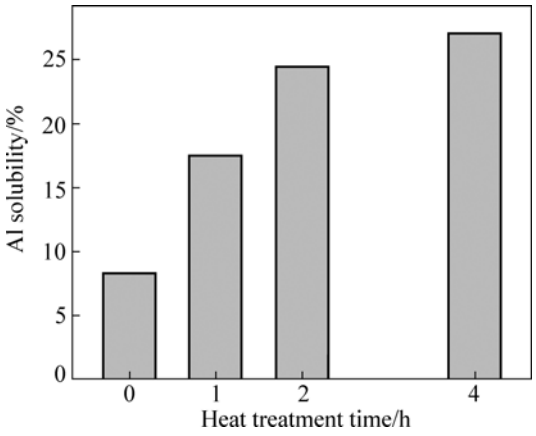

Fig.12 Variation of Al solubility in α matrix of Al-rich surface layer with heat treatment time

Fig.13 shows the corrosion rates of the Al-rich surface layers heat treated for different durations. It can be seen that the corrosion resistance is significantly improved when being heated for 1 h. As discussed above, this is attributed to the increase of the Al solubility in the matrix and the uniform distribution of the β phase particles (Fig.11(a)). Compared with the thixoformed AZ91D alloy and the non-heat-treated Al-rich surface layer, the corrosion resistances are increased by 45% and 30% respectively. But the corrosion resistance is obviously decreased when the heating duration is prolonged and it is even lower than that of the non-heat-treated Al-rich surface layer when being heated for 4 h. This results from the significant agglomeration of the β phase. This result implies that the benefit for the corrosion resistance from the increase of the Al solubility is inferior to the harm from the agglomeration of β phase. So, it can be concluded that in order to improve corrosion resistance, increasing the amount and improving the distribution uniformity of Al-rich phase are more effective than increasing the Al solubility in the matrix.

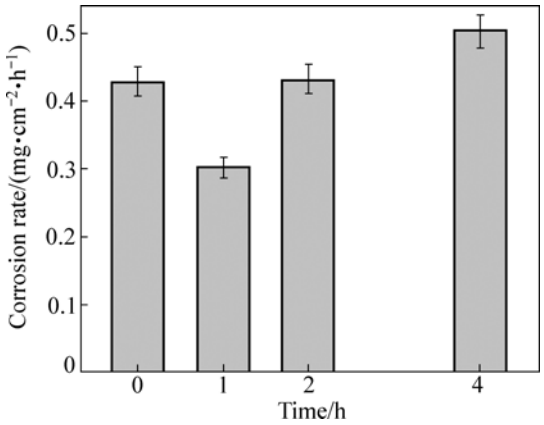

Fig.13 Corrosion rates of Al-rich surface layer solution-treated at 415 ℃ for different times

4 Conclusions

1) Some important information about microstructural evolution of the TMAZ during FSP can be easily obtained by studying the thixoformed AZ91D alloy. The dynamic recrystallization and mechanical separation are the main mechanisms of grain refinement.

2) Compared with the PMC alloy, the microstructural evolution of the TF alloy is slower because the operation efficiency of the grain refinement mechanisms is relatively low. The resulting grain size of the TF alloy is also larger at a given stir pass. But this difference decreases with the increase of stir pass.

3) An Al-rich surface layer can be produced on the thixoformed alloy by FSP and the corrosion resistance in NaCl aqueous solution is obviously improved. The residual pure Al phase in the surface layer can transform into β phase during solution heat treatment.

4) A proper solution heat treatment (at 415 ℃ for 1 h) can further increase the corrosion resistance of the Al-rich surface layer. Increasing the amount and improving the distribution uniformity of the Al-rich phase are more effective than increasing the Al solubility in the matrix for increasing corrosion resistance.

References

[1] ELIEZER D, AGHION E, FROES F H. Magnesium science, technology and applications [J]. Adv Perform Mater, 1998, 5: 201−212.

[2] CZERWINSKI F, ZIELINSKA-LIPIEC A, PINET P J, OVERBEEKE J. Correlation of the microstructure and tensile properties of a thixomolded AZ91D magnesium alloy [J]. Acta Mater, 2001, 49: 1225−1235.

[3] CZERWINSKI F, ZIELINSKA-LIPIEC A. The melting behavior of extruded Mg-8%Al-2%Zn alloy [J]. Acta Mater, 2003, 51: 3319−3332.

[4] LU Y Z, WANG Q D, DING W J. Fracture behavior of AZ91 magnesium alloy [J]. Mater Lett, 2000, 44: 265−268.

[5] TAKUDA H, ENAMI T, KUBOTA K. The formability of a thin sheet of Mg-8.5Li-1Zn alloy [J]. J Mater Process Technol, 2000, 101: 281−286.

[6] KIM H K, KIM W J. Microstructural instability and strength of an AZ31 Mg alloy after severe plastic deformation [J]. Mater Sci Eng A, 2004, 385: 300−308.

[7] MATHIEU S, RAPIN C, HAZAN J, STEINMETZ P. Corrosion behaviour of high pressure die-cast and semi-solid cast AZ91D alloys [J]. Corros Sci, 2002, 44: 2737−2756.

[8] SONG G, ATRENS A. Corrosion mechanisms of magnesium alloys [J]. Adv Eng Mater, 1999, 1: 11−33.

[9] SONG G, ATRENS A, WU X L, ZHANG B. Corrosion behavior of AZ21, AZ501 and AZ91D in sodium chloride [J]. Corros Sci, 1998, 40: 1769−1791.

[10] SONG G, ATRENS A, DARGUSCH M. Influence of microstructure on the corrosion of die cast AZ91D [J]. Corros Sci, 1999, 41: 249−273.

[11] CHARIT I, MISHRA R S. Low temperature superplasticity in a friction-stir-processed ultrafine grained Al-Zn-Mg-Sc alloy [J]. Acta Mater, 2005, 53: 4211−4223.

[12] MISHRA R S, MAHONEY M W, MCFADDEN S X, MARA N A, MUKHERJEE A K. High strain rate superplasticity in a friction stir processed 7075 Al alloy [J]. Scripta Mater, 2000, 42:163−168.

[13] CHANG C I, DUA X H, HUANG J C. Achieving ultrafine grain size in Mg-Al-Zn alloy by friction stir processing [J]. Scripta Mater, 2007, 57: 209−212.

[14] DU X H, WU B L. Using friction stir processing to produce ultrafine-grained microstructure in AZ61 magnesium alloy[J]. Trans Nonferrous Met Soc China, 2008, 18: 562−565.

[15] SATO Y S, PARK S H C, MATSUNAGA A, HONDA A, KOKAW H. A novel production for highly formable Mg alloy plate [J]. J Mater Sci, 2005, 40: 637−642.

[16] CAVALIERE P, DE MARCO P P. Superplastic behaviour of friction stir processed AZ91 magnesium alloy produced by high pressure die cast [J]. J Mater Process Technol, 2007, 184: 77−83.

[17] HSU C J, CHANG C Y, KAO P W, HO N J, CHANG C P. Al-Al_3Ti nanocomposites produced in situ by friction stir processing [J]. Acta Mater, 2006, 54: 5241−5249.

[18] HSU C J, KAO P W, HO N J. Ultrafine-grained Al-Al_2Cu composite produced in situ by friction stir processing [J]. Scripta Mater, 2005, 53: 341−345.

[19] CHUANG C H, HUANG J C, HSIEH P J. Using friction stir processing to fabricate MgAlZn intermetallic alloys [J]. Scripta Mater, 2005, 53: 1455−1460.

[20] HSU C J, KAO P W, HO N J. Intermetallic-reinforced aluminum matrix composites produced in situ by friction stir processing [J]. Mater Lett, 2007, 61: 1315−1318.

[21] DIXIT M, NEWKIRK J W, MISHRA R S. Properties of friction stir-processed Al 1100-NiTi composite [J]. Scripta Mater, 2007, 56: 541−544.

[22] MISHRA R S, MA Z Y, CHARIT I. Friction stir processing: A novel technique for fabrication of surface composite [J]. Mater Sci Eng A, 2003, 341: 307−310.

[23] MORISADA Y, FUJII H, NAGAOKA T, FUKUSUMI M. Effect of friction stir processing with SiC particles on microstructure and hardness of AZ31[J]. Mater Sci Eng A, 2006, 433: 50−54.

[24] LEE C J, HUANG J C, HSIEH P J. Mg based nano-composites fabricated by friction stir processing [J]. Scripta Mater, 2006, 54: 1415−1420.

[25] MORISADA Y, FUJII H, NAGAOKA T, FUKUSUMI M. Nanocrystallized magnesium alloy-uniform dispersion of C_{60} molecules [J]. Scripta Mater, 2006, 55: 1067−1070.

[26] MORISADA Y, FUJII H, NAGAOKA T, FUKUSUMI M. MWCNTs/AZ31 surface composites fabricated by friction stir processing [J]. Mater Sci Eng A, 2006, 419: 344−348

[27] MORISADA Y, FUJII H, NAGAOKA T, NOGI K, FUKUSUMI M. Fullerene/A5083 composites fabricated by material flow during friction stir processing [J]. Composites: Part A, 2007, 38: 2097−2101.

[28] LI Yuan-dong. Study on thixoforming technology, heat treatment and mechanical properties of AZ91D magnesium alloy [D]. Lanzhou: Lanzhou University of Technology, 2005: 81−89. (in Chinese)

[29] CHEN T J, MA Y, LI B, LI Y D, HAO Y. Wear behavior of thixoformed AZ91D magnesium alloy: A comparison with permanent mould cast alloy [J]. Mater Sci Eng A, 2007, 445/446: 477−485.

[30] CHEN Ping-chang, ZHU Li-mei, LI Zan. Forming theory of metal materials [M]. Beijing: China Machine Press, 2003: 105−106. (in Chinese)

[31] MA Z Y. Friction stir processing technology: A review [J]. Metall Mater Trans A, 2008, 39: 642−658.

[32] CHEN T J, MA Y, LI B, LI Y D, HAO Y. Effects of processing parameters on wear behaviors of thixoformed AZ91D magnesium alloys [J]. Mater Des, 2009, 30: 235−244.

(Edited by YANG Bing)